[O III] emitters in the field of the MRC 0316–257 protocluster

F. Maschietto,[1]★ N. A. Hatch,[1] B. P. Venemans,[2] H. J. A. Röttgering,[1] G. K. Miley,[1]
R. A. Overzier,[3] M. A. Dopita,[4] P. R. Eisenhardt,[5] J. D. Kurk,[6] G. R. Meurer,[7]
L. Pentericci,[8] P. Rosati,[9] S. A. Stanford,[10,11] W. van Breugel[11,12] and A. W. Zirm[1,7]

[1]*Leiden Observatory, Leiden University, Niels Bohrweg 2, 2333 CA Leiden, the Netherlands*
[2]*Institute of Astronomy, Madingley Road, Cambridge CB3 OAH*
[3]*Max-Planck-Institut für Astrophysik, Karl-Schwarzschild-Str. 1, D-85741 Garching, Germany*
[4]*Research School of Astronomy & Astrophysics, Australian National University, Cotter Rd., Weston Creek, ACT 2611, Australia*
[5]*Jet Propulsion Laboratory, California Institute of Technology, MS169-327, 4800 Oak Grove Drive, Pasadena, CA 91109, USA*
[6]*Max-Planck-Institut für Astronomie, D-69117 Heidelberg, Germany*
[7]*Department of Physics and Astronomy, Johns Hopkins University, Baltimore, MD 21218, USA*
[8] *INAF–Osservatorio Astronomico di Roma, via Frascati 33, 00040 Monteporzio, Italy*
[9]*European Southern Observatory, Karl-Schwarzschild-Strasse 2, D-85748 Garching, Germany*
[10]*University of California, Davis, CA 95616, USA*
[11]*Institute of Geophysics and Planetary Physics, Lawrence Livermore National Laboratory, Livermore, CA 94551, USA*
[12]*University of California, Merced, PO Box 2039, Merced, CA 95344, USA*

ABSTRACT

Venemans et al. found evidence for an overdensity of Lyα emission-line galaxies associated with the radio galaxy MRC 0316−257 at $z = 3.13$ indicating the presence of a massive protocluster. Here, we present the results of a search for additional star-forming galaxies and active galactic nucleus (AGN) within the protocluster. Narrow-band infrared imaging was used to select candidate [O III] emitters in a 1.1×1.1 Mpc^2 region around the radio galaxy. 13 candidates have been detected. Four of these are among the previously confirmed sample of Lyα galaxies, and an additional three have been confirmed through follow-up infrared spectroscopy. The three newly confirmed objects lie within a few hundred km s^{-1} of each other, but are blueshifted with respect to the radio galaxy and Lyα emitters by $\sim$2100 km s^{-1}. Although the sample is currently small, our results indicate that the radio-selected protocluster is forming at the centre of a larger, $\sim$60 comoving Mpc superstructure. On the basis of a *Hubble Space Telescope*/Advanced Camera for Surveys (*HST*/ACS) imaging study we calculate dust-corrected star formation rates and investigate morphologies and sizes of the [O III] candidate emitters. From a comparison of the star formation rate derived from *UV* continuum and [O III] emission, we conclude that at least two of the [O III] galaxies harbour an AGN which ionized the O$^+$ gas.

Key words: galaxies: active – galaxies: clusters: general – galaxies: evolution – cosmology: observations – early Universe.

1 INTRODUCTION

To understand the formation and evolution of galaxy clusters, it is desirable to find and study their high-redshift progenitors. Although galaxy clusters have been found out to a redshift of $z = 1.5$ (Mullis et al. 2005; Stanford et al. 2005), their higher redshift progenitors are sparse and difficult to find. A successful technique for finding more distant structures that by-passes the need for surveying very large areas of the sky is to search for emission-line galaxies in the neighbourhood of luminous high-redshift radio galaxies (HzRGs) using narrow-band imaging. Multiwavelength studies of HzRGs have resulted in strong evidence that they are massive forming galaxies (e.g. Villar-Martín et al. 2006; Seymour et al. 2007) and are frequently associated with overdensities of emission-line galaxies (Venemans et al. 2007). These overdense regions in the early Universe are the likely progenitors of local galaxy clusters or groups and are termed 'protoclusters'. PROCESS (PROtoCluster Evolution Systematic Study) is a project designed to use a few key radio-selected protoclusters with $2 \leq z \leq 5$ to investigate the formation

★E-mail: maschietto@strw.leidenuniv.nl

and evolution of various populations of galaxies in dense environments (Miley et al. 2004; Venemans et al. 2005, 2007; Overzier et al. 2006, 2008).

This paper presents observations of the protocluster surrounding the PROCESS radio galaxy MRC 0316−257. The associated 1.5-Jy radio source was listed in the 408-MHz Molonglo Reference Catalogue (Large et al. 1981) and was optically identified with a galaxy at $z = 3.13$ by McCarthy et al. (1990). Le Fevre et al. (1996) spectroscopically confirmed two Lyα emitting companions to the HzRG, indicating that the radio galaxy is located in a dense environment. Recently, Venemans et al. (2005, 2007) confirmed 31 Lyα emitters at a similar redshift of MRC 0316−257. The corresponding overdensity is approximately 3.3 times the galaxy field density at this redshift. The protocluster redshift of $z \sim 3.13$ corresponds to an epoch when both the cosmic star formation rate (SFR) and the quasar luminosity function were at their peak, indicating that this is a key epoch for studying the evolution of different populations of galaxies. We have identified and studied additional galaxies in the MRC 0316−257 protocluster on the basis of their redshifted [O III] emission. The observations that we shall discuss here consist of infrared imaging and spectroscopy with ESO's (European Southern Observatory) Very Large Telescope (VLT) and deep optical imaging with the Advanced Camera for Surveys (ACS) on the *Hubble Space Telescope* (*HST*).

Section 2 of this paper is an outline of the observations and the data reduction. In Section 3 we present results from the VLT search programme and the deep ACS images. Corrected SFRs derived from the *UV* fluxes are used to discriminate between star-forming galaxies and obscured active galactic nuclei (AGNs) and the morphologies and sizes of the candidate emitters are discussed. The implications of our results for the space density of [O III] emitting galaxies and the origin of the [O III] emission are discussed in Section 4 and the conclusions of the paper are presented in Section 5. We assume a flat cosmology with $H_0 = 71 \, \text{km} \, \text{s}^{-1} \, \text{Mpc}^{-1}$ and $\Omega_\text{m} = 0.27$ (Spergel et al. 2003). At the distance of MRC 0316−257 an angular scale of 1 arcsec corresponds to a projected linear scale of 7.73 kpc. All magnitudes are given in the AB system (Oke 1974).

2 OBSERVATIONS DATA REDUCTION AND SAMPLE SELECTION

2.1 Infrared narrow-band imaging and selection of [O III] emitting candidates

To search for [O III] emitting galaxies near MRC 0316−257, narrow- and broad-band imaging were carried out between 2003 November and 2004 October in service mode with Infrared Spectrometer and Array Camera (ISAAC; Moorwood et al. 1998) on the 8.2-m ESO VLT Antu (UT1). The pointing was chosen to include the radio galaxy and as many of the confirmed Lyα emitters from Venemans et al. (2005) as possible. The ISAAC narrow-band filter used was NB_2.07, with a central wavelength (λ_c) of 2.07 μm and a width (λ_FWHM) of 0.026 μm. This is sensitive to [O III] emission at redshifts of $z \sim 3.09$–3.16. Broad-band images were obtained to provide an 'off-band' measurement and the magnitude and slope of the continuum emission from candidate line emitters. These were taken in the filters J ($\lambda_\text{c} = 1.25$ μm and $\lambda_\text{FWHM} = 0.29$ μm) and K_s ($\lambda_\text{c} = 2.16$ μm and $\lambda_\text{FWHM} = 0.27$ μm). The detector was a Hawaii array with 1024 × 1024 pixel. The pixel scale was 0.148 arcsec pixel^{-1} and the field-of-view 152 × 152 arcsec^2. The images were taken using dithered exposures of length 150, 75 and 183 s in J, K_s and the narrow-band, each with subintegrations of 30, 15 and 61 s to avoid overexposure

of the background. The total exposure times were 5.3 h each in J and K_s, and 6.9 h in the narrow-band. Standard stars were observed for the photometric calibration. The observed standards include FS6, FS11 and P565C taken from the United Kingdom Infrared Telescope (UKIRT) Faint Standards Catalogue (Hawarden et al. 2001) and S363D from the Las Campanas Observatory (LCO)/Palomar Near Infrared Camera and Multi-Object Spectrometer (NICMOS) Photometric Standards list (Persson et al. 1998).

The images were reduced using the Experimental Deep Infrared Mosaicing Software (XDIMSUM).[1] The effective area of the reduced images was 139 × 139 arcsec^2, and the seeing, as measured from bright stars in the field, was 0.45 arcsec in the NB_2.07 image and 0.55 arcsec in the J and K_s images. The magnitude zero-point of the broad-band images obtained from the various standard star observations has an accuracy of 0.01 mag (J) and 0.03 mag (K_s). The zero-point of the narrow-band image was derived using 52 objects that were detected at a signal-to-noise ratio of at least 20 in both J and K_s. Narrow-band magnitudes were computed for the 52 objects assuming a power-law spectral energy distribution and with the associated counts in the narrow-band image the zero-point was derived with an accuracy of 0.01 mag. The 5σ limiting magnitudes per square arcsec were 23.9 (NB2_2.07), 25.6 (J) and 24.7 (K_s). Objects in the images were extracted using the program SEXTRACTOR (Bertin & Arnouts 1996). The NB_2.07 image was used as the detection image, and aperture photometry was subsequently performed on both the narrow- and broad-band images. For detection, objects were required to have a signal-to-noise ratio of >5 in the NB_2.07 image. The colours of the detected objects were measured in circular apertures, while the 'total' flux was measured in an elliptical aperture. A total of 143 objects having a signal-to-noise ratio of at least 5 were detected in the narrow-band image. Following Kurk et al. (2004), we select objects with a rest-frame equivalent width $\text{EW}_0 > 50 \, \text{Å}$ and a significance $\Sigma \equiv \text{EW}_0 / \Delta \text{EW}_0 > 3$ as candidate [O III] emitters (see Venemans et al. 2005 for more details on the object detection and photometry and on how EW_0 and ΔEW_0 are computed). Each candidate was inspected visually in order to remove spurious sources. This resulted in a list of 17 candidate [O III] emitting galaxies. To remove foreground galaxies with emission lines that fall into the NB_2.07 filter, we measured the colours of the candidates on archival u', V and I images (Venemans et al. 2005, 2007). Three candidates had $u' - V$ colours of <1.2 and are likely foreground objects. Two of the candidates lie very close together and after inspection of the galaxy morphologies were determined to be a single merging object. The spatial distribution of the remaining 13 candidate [O III] emitters is plotted in Fig. 1. One of the candidates is the radio galaxy (ID 1), four are spectroscopically confirmed Lyα emitters (IDs 3, 6, 7, 11), six are likely Lyman break galaxies (LBGs; defined as objects with $u' - V > 1.6$ and $V - I < 0.6$; IDs 2, 3, 4, 7, 8, 10) and two satisfy the selection criteria for distant red galaxies (DRGs; $J - K_\text{s} > 1.4$; IDs 3, 5). For an overview see Table 1.

2.2 ACS optical imaging

We obtained deep images in r_{625} and I_{814} filters with the ACS (Ford et al. 1998) on the *HST*. The MRC 0316−257 protocluster was observed with the ACS during 2004 December 14–31 and 2005 January 2–21 in two 3.4 × 3.4 arcmin^2 ACS fields that overlapped

---

[1] http://iraf.noao.edu/iraf/ftp/iraf/extern/xdimsum/xdimsum.readme
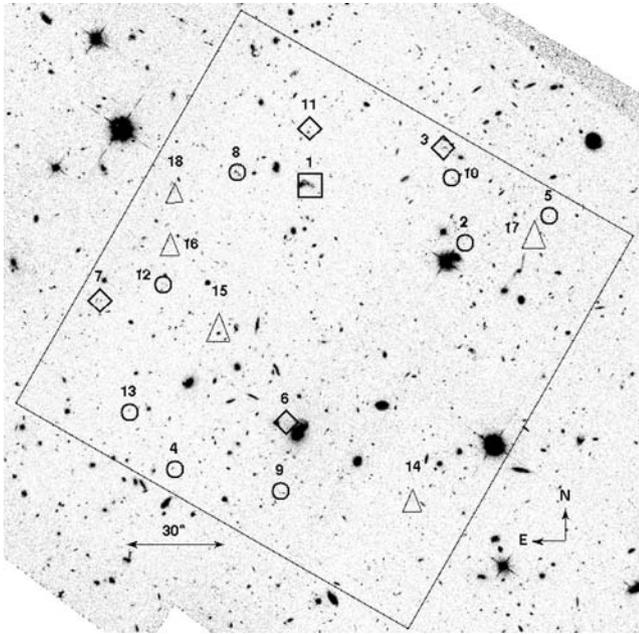
Figure 1. The ACS I_{814} image with the [O III] candidate emitting galaxies marked. The square symbol denotes the radio galaxy, the circles mark the [O III] candidates, the diamonds identify the [O III] candidate emitters which are also confirmed Lyα emitters, the triangles indicate the Lyα galaxies with no detected [O III] emission. The large box indicates the ISAAC field-of-view.

by ∼1 arcmin in a region that includes the radio galaxy. The exposure time per pointing was 22 410 s in I_{814} (10 orbits per pointing) and 11 505 s in r_{625} (five orbits per pointing). The I_{814} images were combined with a 6300-s exposure (three orbits) taken with ACS on 2002 July 18. All observations were processed through the ACS Guaranteed Time Observation (GTO) pipeline (Blakeslee et al. 2003) to produce registered, cosmic-ray rejected images. The extinctions in the direction of the radio galaxy are 0.04 and 0.03 mag at wavelengths corresponding to the r_{625} and I_{814} filters, respectively. In its deepest part (about 1/5 of the image), the 2σ depths are 29.1 (r_{625}) and 29.6 (I_{814}) AB mag, measured in a square 0.45-arcsec diameter aperture. In its shallowest outer part (about 2/5 of the image), the 2σ depths are 28.5 (r_{625}) and 29.3 (I_{814}) mag. The r_{625} and I_{814} filter bands correspond to a central wavelength of ∼1513 and 1937 Å in the rest frame, respectively. We determined the rest-frame *UV* magnitudes and the relative rms errors of the [O III] candidates from the ACS images using SExtractor, cross-checking the results using both circular and elliptical apertures with the IDL routine ATV. All the 13 [O III] candidate emitters were detected in both the *UV* filters with the faintest having a I_{814} magnitude of 26.2.

2.3 Infrared spectroscopy

Infrared spectra of four candidate [O III] emitters were obtained with ISAAC (Moorwood et al. 1999) at the ESO VLT Antu (UT1) on the nights of 2006 August 31, September 3 and November 23. The observations used the short wavelength camera of ISAAC and the medium resolution grating, resulting in a pixel scale of 0.148 arcsec and a spectral dispersion of 1.23 Å. The observations were carried out under variable optical seeing conditions, which were typically between 0.8 and 1 arcsec, except for the final part of the night of September 3, where the seeing was ∼0.33 arcsec. The 1×120 arcsec^2 slit was employed in all cases, except for a 90-

min observation on the night of September 3, when the slit width was changed to 0.6 arcsec. The 1×120 arcsec^2 slit resulted in a resolution of 7.4 Å FWHM (or $R \sim 2600$).

The target galaxies were acquired using the imaging mode of ISAAC. The [O III] galaxies are faint so the slit was first centred on a nearby bright star with $17.6 \leq K_{AB} \leq 19.8$ and then offset to the target galaxies. High precision is required for determining the coordinates of the [O III] emitters. However, the reduced ISAAC NB_2.07, *J*- and K_s-band images that were used for the candidate selection have poor astrometric accuracy due to the low number of reference stars in the field. Therefore, a *I*-band FORS (Focal Reducer/low dispersion Spectrograph) image of the field, earlier obtained (Venemans et al. 2005), was used to determine the required offsets.

Four candidate [O III] emitters were observed, galaxies identified as 2, 4, 5 and 9 in Fig. 1. The exposure time for candidates IDs 5 and 2 was 19 800 s and for IDs 4 and 9 was 18 000 s. We employed the classical ABBA sequence to remove the sky background and sky emission lines. The exposure time for each integration was either 600 or 900 s. All observations were carried out at airmass smaller than 1.7. A set of xeon and argon arc spectra was taken during each observing night for wavelength calibration.

The data were reduced using the ISAAC data reduction software package ECLIPSE, which is available from ESO. The data were flat-fielded and the arcs were used to model and remove the slit curvature, and wavelength calibrates the data. The arcs from the night of 2006 November 23 contained 14 detected arclines and the standard deviation of the fit was 0.2 Å, whereas on the nights of 2006 August 31 and September 3 there were 12 and 11 lines detected with a standard deviation of 0.4 and 0.5 Å, respectively. The wavelength of the skylines was measured to check the arc calibration. No deviations greater than 0.6 Å were found. The sky background and night sky emission lines were removed by the ABBA dither sequence, however a feature at 2.041 μm had prominent residuals and has been masked out in the spectra shown in Fig. 2.

3 RESULTS

3.1 Redshift distribution

The spectra of the [O III] galaxies are presented in Fig. 2 together with the night sky emission-line spectrum. Three of the four targets (IDs 2, 4 and 5) exhibit a strong [O III]λ λ5007, 4959 emission-line doublet shifted into the window $3.095 \leq z \leq 3.105$. The presence of both lines of the [O III]λ λ5007, 4959 doublet in these spectra confirm that the selected targets are [O III] emitters. Table 1 lists the redshifts of the three confirmed [O III] emitters, the radio galaxy MRC 0316−257 and the four [O III] candidates, that are also Lyα emitting galaxies spectroscopically confirmed to be members of the MRC 0316−257 protocluster. Fig. 3 shows the redshift distribution of the spectroscopically confirmed [O III] emitting galaxies together with the redshift distribution of the spectroscopically confirmed Lyα emitting galaxies that comprise part of the protocluster around MRC 0316−257. The redshifts of the Lyα emitting galaxies are taken from Venemans et al. (2005). They were selected using a narrow-band filter sensitive to the redshift range 3.12–3.17.

The three spectroscopically confirmed [O III] emitting galaxies occupy a narrow range in velocity distribution, although their redshifts falls ∼2100 km s^{-1} blueward of the mean redshift of the MRC 0316−257 protocluster.

Although one candidate [O III] emitter (ID 9) was not detected, this non-detection is not significant. The object is almost a factor of

Table 1. Properties of the [O III] emitters in the field together with confirmed Lyα emitters within the ISAAC field-of-view. Column 1 gives the assigned source numbers and columns 2 and 3 the equatorial celestial coordinates, respectively, right ascension and declination. Columns 4 and 5 give the [O III] and Lyα fluxes in units of 10^{-17} erg s^{-1} cm^2, errors are at 1σ. Lyα fluxes are determined from same apertures as [O III] fluxes. The [O III] flux given in column 4 for these galaxies is a 2σ upper limit. The redshifts are given in column 6 and the line used to obtain them is specified as subscript. The visual magnitudes are shown in column 7. Column 8 gives the comments about the galaxy types where the label RG indicates the radio galaxy, LAE indicates the galaxy is a spectroscopically confirmed Lyα emitting galaxy in the protocluster, DRG indicates the galaxy is a candidate 'distant red galaxy' and the label LBG indicates that the galaxy is a candidate Lyman break galaxy at the redshift of the protocluster. Galaxy ID 3 has extended Lyα and [O III] emission. Galaxies IDs 14–18 are not detected in [O III] but are within the ISAAC field-of-view and are spectroscopically confirmed Lyα emitters within the protocluster. Photometry of the radio galaxy is unreliable as it lies very close to a foreground galaxy.

Source ID (1)	RA (J2000) ($^h:^m:^s$) (2)	Dec. (J2000) ($^\circ:':''$) (3)	[O III] flux (10^{-17} erg s^{-1} cm^2) (4)	Lyα flux (10^{-17} erg s^{-1} cm^2) (5)	Redshift (6)	m_V (7)	Comments (8)
1	03:18:12.1	−25:35:10.5	169 ± 1.7	84	$3.131_{Ly\alpha}$	23.8	RG, LBG, DRG, LAE
2	03:18:08.6	−25:35:28.8	39.0 ± 5.1	–	$3.094_{[O\,III]}$	25.3	LBG
3	03:18:09.0	−25:34:59.3	8.7 ± 1.0	18.0	$3.136_{Ly\alpha}$	24.7	LBG, DRG, LAE
4	03:18:15.1	−25:36:37.8	8.5 ± 0.9	–	$3.106_{[O\,III]}$	25.7	LBG
5	03:18:06.6	−25:35:20.1	8.3 ± 1.3	–	$3.104_{[O\,III]}$	26.4	DRG
6	03:18:12.6	−25:36:23.0	5.9 ± 0.9	4.6	$3.123_{Ly\alpha}$	–	LAE
7	03:18:16.8	−25:35:46.1	4.3 ± 0.9	6.3	$3.131_{Ly\alpha}$	24.9	LBG, LAE
8	03:18:13.7	−25:35:07.7	4.2 ± 0.8	–	–	23.9	LBG
9	03:18:12.7	−25:36:44.4	2.4 ± 0.7	–	–	26.9	–
10	03:18:08.8	−25:35:08.3	2.3 ± 0.5	–	–	25.7	LBG
11	03:18:12.0	−25:34:52.9	2.3 ± 0.6	1.5	$3.141_{Ly\alpha}$	26.5	LAE
12	03:18:15.3	−25:35:41.1	1.5 ± 0.4	–	–	–	–
13	03:18:16.1	−25:36:19.9	1.3 ± 0.4	–	–	25.3	–
14	03:18:09.7	−25:36:47.5	<1.1	2.9	3.124	–	LAE
15	03:18:14.1	−25:35:54.3	<1.2	1.1	3.132	–	LAE
16	03:18:15.2	−25:35:28.9	<0.5	1.0	3.146	–	LAE
17	03:18:06.9	−25:35:26.2	<0.7	0.8	3.143	–	LAE
18	03:18:15.1	−25:35:13.1	<0.7	0.72	3.131	–	LAE

4 fainter than the faintest spectroscopically detected galaxy and its narrow-band flux would only have resulted in a marginal detection in the available spectroscopic exposure time.

3.2 Extinction-corrected star formation rates of the [O III] emission-line galaxies

3.2.1 Star formation rates from UV continuum

Under the assumption that the galaxies are dominated by hot, young massive stars and are relatively dust free, one can use the luminosity of the *UV* continuum to estimate a SFR. We convert the r_{625} magnitudes of the [O III] candidates into a SFR using

$$\begin{aligned} \text{SFR } \left(M_\odot\, yr^{-1} \right) &= \frac{4\pi D_L^2 F_\nu}{(1+z)8\times 10^{27}\left(erg\,cm^{-2}\,s^{-1}\,Hz^{-1}\right)} \\ &= \frac{L\,(1500\,\text{Å})}{8\times 10^{27}\left(erg\,s^{-1}\,Hz^{-1}\right)} \end{aligned} \tag{1}$$

for a Salpeter initial mass function (IMF), where D_L^2 is the luminosity distance and $F_\nu = 10^{[-0.4(r_{AB}+48.6)]}$ the flux density (Madau, Pozzetti & Dickinson 1998). We determine a reddening correction from the *UV* continuum slope, derived from the measured $r_{625} - I_{814}$ colour. We assume the galaxies have a standard power-law spectrum with slope β ($F_\lambda \propto \lambda^\beta$), so that a spectrum that is flat in F_ν has $\beta = -2$. We define

$$\beta_{rI} = -0.4\frac{(r_{625} - I_{814})}{\log_{10}(\lambda_r/\lambda_I)} - 2, \tag{2}$$

where λ_r and λ_I are the central wavelengths of the r_{625} and I_{814} ACS filters. In general, we note that the *UV* slope β gives a reasonable

estimate for the extinction if the object has a 'pure' starburst spectrum and is not a mix of old and new populations (Kong et al. 2004). We determine the extinction through

$$E(B-V) = \frac{\beta - \beta_0}{8.067}, \tag{3}$$

with $\beta_0 = -2.5$, as expected for ionizing populations (Meurer et al. 1995). The β_0 changes somewhat as a function of age and which part of the *UV* spectrum is being used to estimate the slope. Meurer & Heckman (1995) derived β_0 from a fit to the *UV* spectrum over the wavelength range that we approximate here with $r_{625} - I_{814}$. A wide range of star formation histories, from short bursts less then 10-Myr old to continuous star formation 100 Myr and older will produce a spectrum with $\beta_0 \approx -2.5$. The range in $\beta_0 = -2.5$ of ± 0.2 for ionizing populations amounts to an uncertainty in obscuration $A(1500)$ of ± 0.21 mag. We derive the obscuration at 1500 Å [$A(1500)$] using the correlation in Calzetti et al. (2000):

$$A(1500) = 4.39\,E(B-V), \tag{4}$$

although we note that this correlation has a relative large scatter. We present the extinction-corrected *UV* SFRs in Table 2.

We do not include the *UV* continuum and [O III] SFRs for the radio galaxy because the photometry is unreliable as it lies very close to a luminous foreground galaxy. However, we note that the *UV* continuum of the radio galaxy is dominated by emission from stars. The contribution from scattered AGN light is limited by the upper limit on the polarization of the continuum of $P < 4$ per cent (De Breuck & Reuland 2005). If all the light at a rest frame of 1500 Å is due to young stars, the SFR of the radio galaxy is $\sim 100\,M_\odot\,yr^{-1}$ (uncorrected for dust absorption). This is similar to the uncorrected
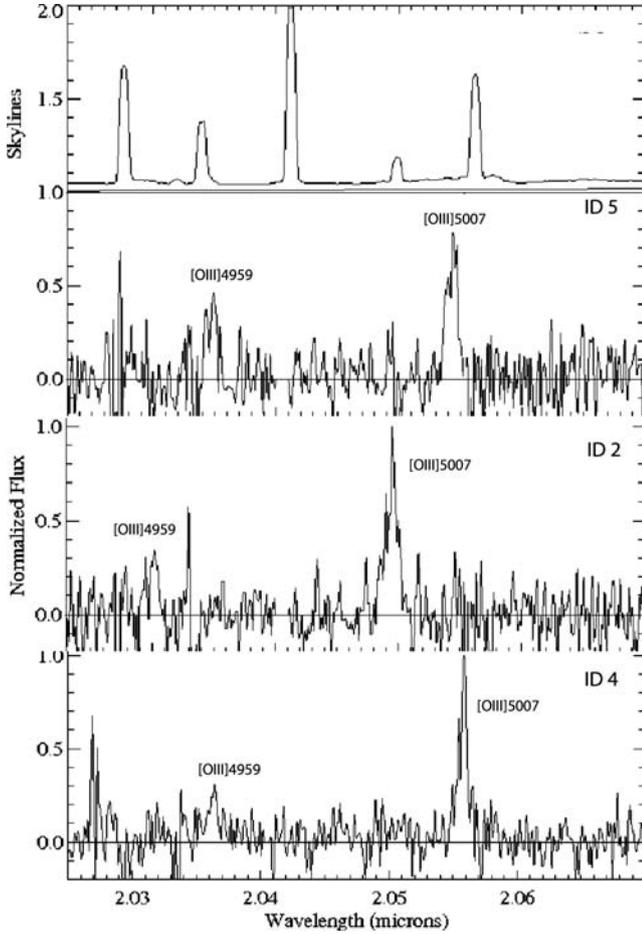
Figure 2. One-dimensional spectra of the three confirmed [O III] emitters together with the night emission skylines. The [O III]λ λ5007, 4959 doublet lines are both clearly visible in each spectrum. A residual emission-line feature at 2.04 μm has been mashed out.
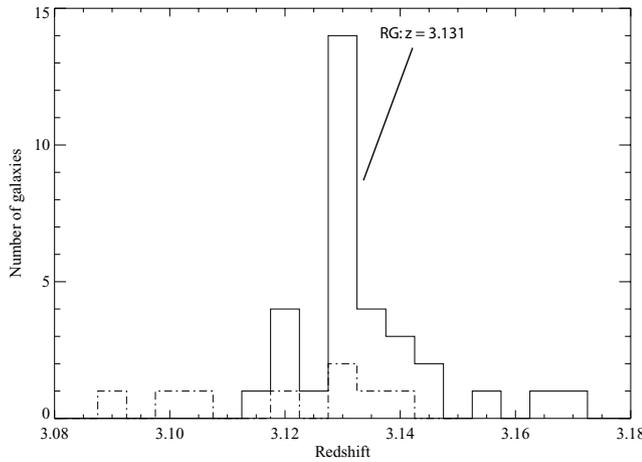

Figure 3. Redshift histogram of the spectroscopically confirmed [O III] emitters (dash–dotted line) together with the previously known 32 Lyα emitters (solid line). Lyα emitters also include the radio galaxy.

SFRs in radio galaxies at $z \sim 2.5$ (Vernet et al. 2001) as calculated from the rest-frame *UV* continuum. However, the calculated SFR is likely to be a lower limit because radio galaxies are known to have significant amounts of obscured star formation (Stevens et al. 2003).

3.2.2 Star formation rates from [O III] emission

Kennicutt (1992) demonstrated that the large dispersion in the [O III]/Hα ratio among star-forming galaxies makes [O III] an unsuitable emission line for determining SFRs. The large dispersion is dominated by the variation in excitation mechanism and oxygen abundance, as well as reddening (Moustakas, Kennicutt & Tremonti 2006). However, Moustakas et al. (2006) note that [O III] can be used to make a crude estimate of the SFR and in particular can be used to estimate minimum SFRs. Fig. 13 from Moustakas et al. (2006) shows that there is a maximum [O III]/Hα ratio observed from star-forming galaxies which is ~ 2.4 (Teplitz et al. 2000). Using this maximum ratio and the conversion between Hα and SFR from Kennicutt (1998):

$$\mathrm{SFR}_{\mathrm{H\alpha}}\ (\mathrm{M}_\odot\ \mathrm{yr}^{-1}) = 7.9 \times 10^{-42} \frac{L_{\mathrm{H\alpha}}}{\mathrm{erg\ s}^{-1}}, \tag{5}$$

we derived a lower limit to the SFR from the [O III] luminosity to be

$$\mathrm{SFR}_{[\mathrm{O\,III}]}\ (\mathrm{M}_\odot\ \mathrm{yr}^{-1}) > 0.33 \times 10^{-41} \frac{L_{[\mathrm{O\,III}]}}{\mathrm{erg\ s}^{-1}}. \tag{6}$$

We note that the extinction derived from the ionized gas (Fanelli, O'Connell & Thuan 1988) is not the same as the extinction derived from the *UV* stellar continuum (Calzetti & Heckman 1999; Calzetti et al. 2000). We have therefore used the calibration from Calzetti et al. (2000) linking the stellar continuum colour excess to the colour excess derived from the nebular gas emission lines:

$$E(B-V)_{\mathrm{stars}} = (0.44 \pm 0.03) E(B-V)_{\mathrm{gas}}. \tag{7}$$

We determined the intrinsic [O III] line flux through

$$F_{\mathrm{i}}(\lambda) = F_{\mathrm{o}}(\lambda) 10^{0.4 E(B-V)_{\mathrm{gas}} k'(\lambda)}, \tag{8}$$

where $F_{\mathrm{i}}(\lambda)$ and $F_{\mathrm{o}}(\lambda)$ are the intrinsic and observed [O III] line flux densities, respectively, and $k'(\lambda)$ is defined as $k'(\lambda) = A'(\lambda)/E(B-V)_{\mathrm{gas}}$ and given by

$$k'(\lambda) = 2.659(-2.156 + 1.509/\lambda - 0.198/\lambda^2 + 0.011/\lambda^3) + R'_V,$$
$$0.12 \leq \lambda \leq 0.63\ \mu\mathrm{m}, \tag{9}$$

where λ is 0.5007 μm the rest-frame wavelength of the [O III] emission line, and the default value of R'_V is 4.05 based on comparison with starburst galaxies (Calzetti & Heckman 1999; Calzetti et al. 2000).

We list extinction-corrected [O III] SFRs and the ratio (SFR [O III])/(SFR [*UV*]) in Table 1. This ratio shows that approximately half (7/13) of the candidates have a comparable SFR derived from the *UV* continuum and [O III] emission, whilst 3/13 have a ratio of approximately 7–8, and 2/13 have very high (SFR [O III])/(SFR [*UV*]) ratios. A large discrepancy between the derived SFRs on the basis of *UV* continuum and [O III] emission, i.e. a high (SFR [O III])/(SFR [*UV*]), may indicate a different or additional [O III] excitation source other than star formation. We note that the [O III] SFRs are lower limits as we used the maximum [O III]/Hα ratio of 2.4. Hence the (SFR [O III])/(SFR [*UV*]) may be larger by this factor. Moustakas et al. (2006) show that variations in chemical abundance, ionization parameter and reddening all increase the scatter in the relation between the SFR as derived by Hα emission and [O III] luminosity.

Table 2. Dust-corrected *UV* and [O III] SFRs of the 13 [O III] emitters in the field. Column 1 gives the source IDs. The *UV* SFRs and the [O III] SFRs of the emitters, both corrected for dust obscuration, are shown in columns 2 and 3, respectively. SFRs are given as $M_\odot$ yr^{-1}. Column 4 gives the corrected (SFR [O III])/(SFR [*UV*]) ratios and column 5 the *UV* extinctions for all candidates. Candidate 14–18 (see Table 1), which were not detected in [O III], are not displayed.

Source ID	Corr SFR (*UV*[1550 Å]) ($M_\odot$ yr^{-1})	Corr SFR ([O III]) ($M_\odot$ yr^{-1})	(SFR [O III])/(SFR [*UV*])	$E(B-V)_{UV}$
(1)	(2)	(3)	(4)	(5)
1	439.8	–	–	0.358 ± 0.007
2	9.1	252.8	27.7	0.090 ± 0.032
3	17.1	44.5	2.6	0.061 ± 0.036
4	15.3	122.2	8.0	0.173 ± 0.034
5	5.1	36.1	7.1	0.045 ± 0.088
6	1.4	63.3	45.2	0.141 ± 0.065
7	16.5	22.1	1.4	0.065 ± 0.022
8	150.1	45.1	0.3	0.136 ± 0.065
9	5.1	20.4	4.0	0.124 ± 0.100
10	8.0	14.6	1.8	0.084 ± 0.048
11	5.1	36.2	7.1	0.180 ± 0.062
12	2.4	7.3	3.1	0.055 ± 0.115
13	16.7	20.7	1.2	0.184 ± 0.034

They conclude that the 1σ uncertainty associated with converting the [O III] luminosity into a SFR is a factor of 3–4. We conclude that the [O III] luminosity of only two galaxies (IDs 2 and 6) is beyond that expected from its *UV*-determined star formation with more than 3σ confidence; therefore, they require an additional excitation source – most likely an AGN. We don't quote measurement errors for the SFRs in the tables because they are much smaller than the intrinsic scatter of 3–4 in the conversion.

3.3 Sizes and morphologies of the [O III] emitters

Figs 4–6 show r_{625} and I_{814} 'postage stamp' regions of the 13 [O III] candidates. From a visual inspection approximately half (eight objects) of the [O III] candidate emitters have morphologies characterized as a bright compact core surrounded by diffuse emission with significantly lower surface brightness. The remaining five candidates (including the radio galaxy shown in Fig. 6) have diffuse or clumpy morphologies. These objects have larger sizes and do not posses an obvious core. To quantify the sizes of these objects, the half-light radius (r_h) of each emitter was measured using the program SEXTRACTOR on the I_{814}-band images. The half-light radius is defined as the radius of a circular aperture in which the flux is 50 per cent of the total flux. The half-light radii of the candidates range from 0.06 to 0.75 arcsec. The sizes of the candidate emitters in the I_{814} band are given in Table 3. Galaxies that are diffuse or clumpy have larger uncertainties due to their irregular shapes. The measured physical sizes correspond to 1.2–4.8 kpc. The mean half-light radius of isolated, unsaturated stars in the ACS field was found to be $\sim$0.06 arcsec. One of the [O III] candidates, ID 6, is classified as unresolved. We compared the measured sizes of the confirmed Lyα emitters (IDs 3, 6, 7 and 11) with that of Venemans et al. (2005). The sizes of the confirmed Lyα emitting sources in Venemans et al. (2005) were also derived from the analysis of an ACS image taken within the I_{814} filter, and the half-light radius of
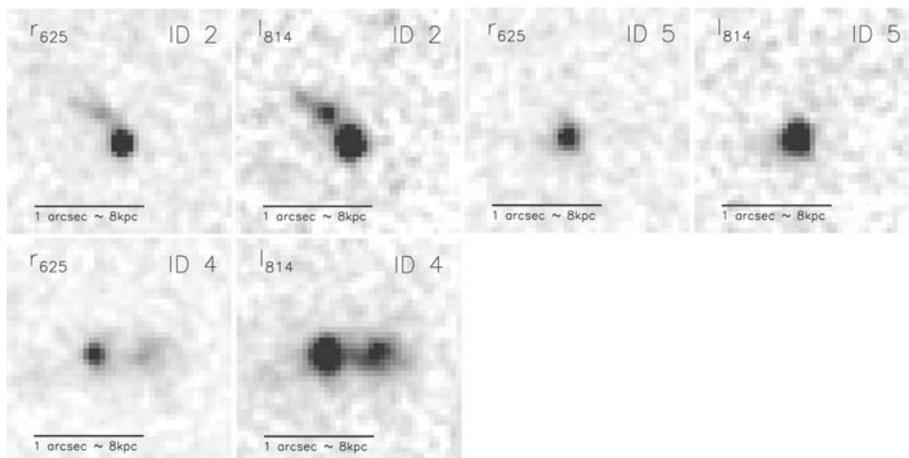

Figure 4. ACS r_{625}-band (left-hand columns) and I_{814}-band (right-hand columns) images of the three confirmed [O III] emitters. From top to bottom: IDs 2, 4 and 5. The scale is 0.05 arcsec pixel^{-1} and each box is 2 arcsec on each side. Only ID 5 has a single component in both *UV* bands. The other two objects instead reveal, most clearly in the *I* band, the presence of a secondary 'core' (ID 2) or of an extended structure (ID 4). The derived corrected SFR for object 2 indicates that it could be an obscured AGN.
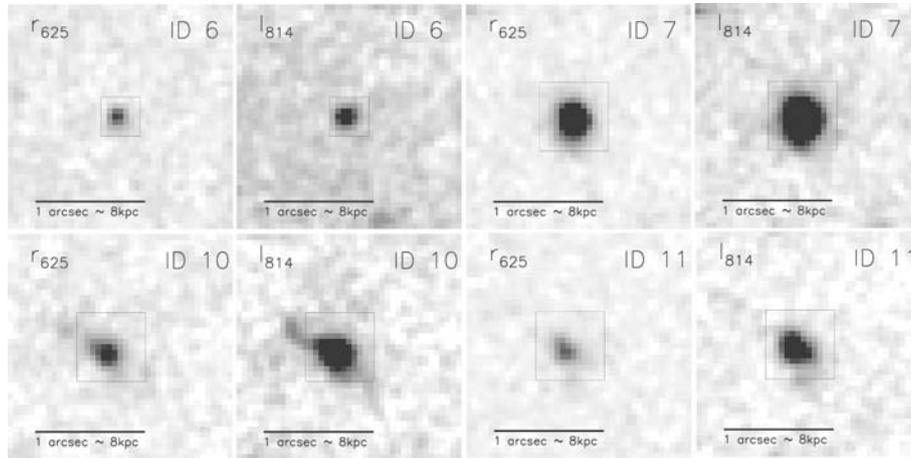
Figure 5. ACS r_{625}-band (left-hand column) and I_{814}-band (right-hand column) images of the four 'compact' [O III] candidates. The scale is 0.05 arcsec pixel^{-1} and each box is 2 arcsec on each side. The detection squares are centred on the detection pixel and their sides match the sizes of the objects (see Section 3.3 and Table 3 for the values). Consistently with the mean half-light radius of unsaturated stars in the ACS field of $\sim$0.09 arcsec we cannot exclude the presence of unresolved components within these 'compact' objects.
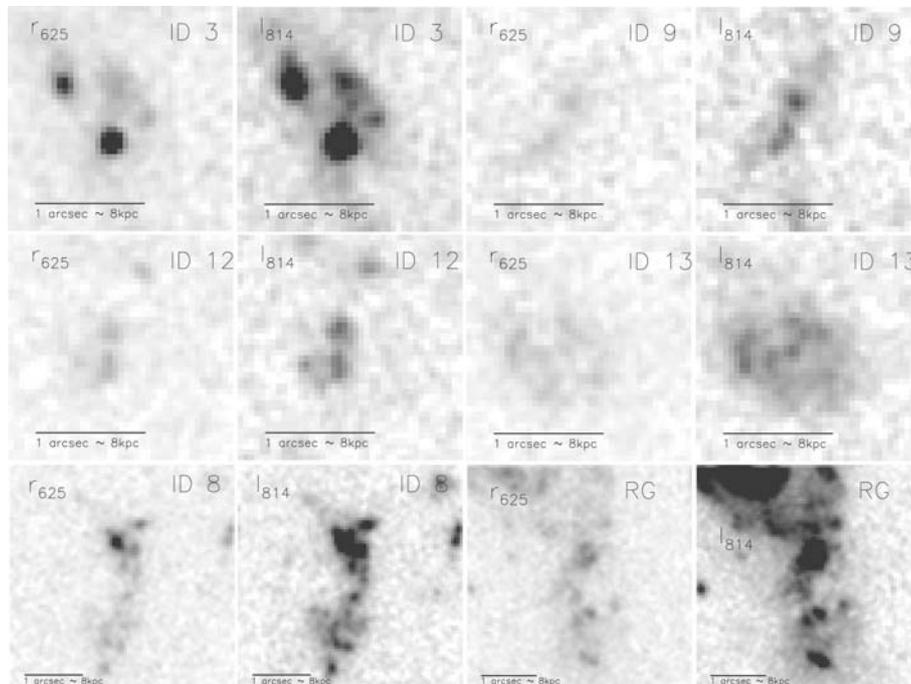

Figure 6. ACS r_{625}-band (first and third columns) and I_{814}-band (second and fourth columns) images of the six 'diffuse and clumpy' objects. The scale is 0.05 arcsec pixel^{-1} and each box is 2 arcsec on each side. The radio galaxy is showed together with object ID 8 (the probable merger) at the bottom row. The dimension of their detection boxes is 4 arcsec. Objects that have larger sizes and are diffuse or clumpy are plotted without the detection squares.

each emitter was measured using the program SExtractor too. We found a good match within an error of $\sim$0.5 kpc. The mean half-light radius of the [O III] emitters is 1.8 kpc, which is comparable to that of luminous LBGs at $z \sim 3$ (Bouwens et al. 2004; Ferguson et al. 2004).

We find a range of morphologies from simple compact to clumpy and diffuse typical of LBGs (Giavalisco et al. 1996; Lotz et al. 2004, 2006; Elmegreen 2007). The ACS image of the radio galaxy shows several objects within 3 arcsec ($\sim$25 kpc), surrounded by low surface brightness emission ($\geq$ 24.8 mag arcsec^{-2}). Such a structure is typical for the rest-frame *UV* emission from the hosts of the most

luminous, radio-loud sources at high redshift (Pentericci et al. 1999; Venemans et al. 2005; Zirm et al. 2005; Miley et al. 2006; Hatch et al. 2008).

Objects IDs 3, 8, 9, 12 and 13 are clumpy with two or three clumps clearly visible in the I_{814}-band image (Fig. 6). They are probably single extended objects with a lot of structure and clumps that we interpret as different regions of star formation, perhaps induced by a galaxy merger. According to Elmgreen et al. (2005) the clumpy objects may not be mergers, but rather unstable discs. Objects IDs 2, 4, 5 and IDs 6, 7, 10 and 11 are identified with single objects in the ACS images (Figs 4 and 5). However, in some cases where the

Table 3. Sizes and morphologies of the [O III] candidate emitters located within the field of ACS. Column 1 gives the source IDs. The half-light radii in arcsec and kpc are given in column 2 and column 3, respectively. Column 4 gives information about the morphology of the emitters. The sizes of the galaxies which are diffuse or are multiple objects have a larger uncertainty in their values because of the irregular shapes. The (*) labels the confirmed Lyα emitters from Venemans et al. (2005). ID 6, having a $r_h \sim 0.06$ arcsec, is unresolved.

Source ID (1)	r_h (arcsec) (2)	r_h (kpc) (3)	Morphology (4)
1	–	–	Clumpy (RG)
2	0.13	∼1.0	Double core
3*	0.26	∼2.0	Clumpy
4	0.27	∼2.1	Double core
5	0.10	∼0.8	Single compact core
6*	0.06	<0.5	Single compact core
7*	0.20	∼1.5	Single compact core
8	0.75	∼5.8	Clumpy
9	0.15	∼1.2	Single core
10	0.17	∼1.3	Single compact core
11*	0.12	∼0.9	Single compact core
12	0.19	∼1.5	Clumpy
13	0.43	∼3.3	Clumpy

objects appear to be single ones in the [O III], the I_{814} images reveal 'double core' (IDs 2, 4, 9 and 10). On average those two cores are separated less than 0.5 kpc from each other.

We note that the compact clumps seen in the *HST* images may contain substructure on a smaller scale than the *HST* resolution, that prevents one from concluding that they have spheroidal or discy morphologies. This can be seen from a comparison with the rest-frame *UV* morphologies of a sample of local analogues of high-redshift LBGs as well as with gravitationally lensed LBGs (Overzier et al. 2008). Both clumpy and compact core-dominated galaxies clearly show extended diffuse emission around or extending from them, which could be an indication of interacting systems (Younger et al. 2007). In a few cases, the [O III] emission coincides with the mean centroid of the *UV* continuum. In other cases, the [O III] emission mainly comes from one of the two components visible in the *UV*. Fig. 6 shows three objects (IDs 3, 9 and 12) that associate the position of the single [O III]-selected candidate with, respectively, a double (IDs 3 and 9) and a triple (ID 12) detection in the ACS *UV* images (most clearly seen in the I_{814}). In all the three cases the detection box gives the position of the candidate as referred in the [O III]-selected list. In summary, the [O III] emitting galaxies show a range of diverse morphologies.

4 DISCUSSION

4.1 Space density of [O III] emitting galaxies

How do the redshifts of galaxies detected on the basis of their redshifted [O III] emission relate to the protocluster at $z = 3.13$ found by Venemans et al. (2005)? At $z > 2.8$, [O III]λ5007 is the most easily observed bright emission line in star-forming galaxies, since Hα is redshifted beyond the near-infrared and Lyα is only present in a small fraction of LBGs (Pettini et al. 1998; Shapley et al. 2003). However, the selection of [O III] emitters at high redshift using narrow-band imaging in the infrared is far less common than similar techniques used to target Lyα or Hα (Moorwood et al. 2000; Teplitz et al. 2000). Consequently, not much is known about the number density and clustering statistics of [O III]-selected objects at $z \sim 3$.

Moorwood et al. (2000) detected five [O III] emitters at redshift 3.1 in an 18.9 arcmin² field with flux greater than 8×10^{-17} erg cm⁻² s⁻¹, consistent with the statistics of one object in 3 arcmin² found by Teplitz, Malkan & McLean (1999) . Including the radio galaxy, we detect 13 candidate [O III] emitters in this field, and we have obtained redshifts for seven of these. Four objects had previously determined redshifts based on Lyα, and are among the protocluster galaxies at $z \approx 3.13$. The remaining three objects were spectroscopically identified as galaxies at $z \approx 3.10$, and have colours consistent with LBGs (objects #2 and #4 in Table 1) and red galaxies (#5). It thus seems likely that the remaining [O III] emitters also have redshifts $z \sim 3.1$. If we constrain our sample to the same limiting depth as obtained by Moorwood et al. (2000), and take into account that our field area is 3.5 times smaller, we obtain a local density in the [O III] field of 3.5 times the field density and finally, according equation (21) in Venemans et al. (2005), a galaxy overdensity of 2.5. If the [O III] emitting galaxies are a subset of the general population of star-forming galaxies at $z \sim 3$, their distribution can be expected not to be random, but relatively strongly clustered both in real space and in velocity space (e.g. Ouchi et al. 2004; Monaco et al. 2005; Lee et al. 2006). This makes it difficult to assess the statistical significance of the apparent enhancement in the observed number density of [O III] emission-line galaxies, without additional observations or a detailed comparison with simulations. Nevertheless, the observed space density of [O III] galaxies is consistent with the overdensity of 2.3 derived for Lyα galaxies in the MRC 0316−257 protocluster by Venemans et al. (2005).

It is interesting to note that the three newly obtained redshifts all have $z \approx 3.10$, compared with $z \approx 3.13$ for the Lyα protocluster. These [O III] emitters appear therefore to be blueshifted by 2100 km s⁻¹ relative to the radio galaxy and its associated protocluster of Lyα emitters. It is unclear whether this apparent shift truly reflects the distribution of the [O III] emitters in this field, or whether it is due to small-number statistics resulting from the ∼50 per cent incompleteness of our spectroscopic follow-up.

It is unlikely that the [O III] lines are systematically shifted with respect to the Lyα line, as the shift of 2100 km s⁻¹ is larger than the typical 600 km s⁻¹ shift that one would expect. The [O III] filter covers a larger redshift range than the Lyα filter, extending to lower redshifts. It is possible that another structure exists at $z \sim 3.10$ which is not detected through Lyα emitters due to the limited range of the Lyα filter. The formal, comoving distance between $z = 3.13$ and 3.10 is ∼30 h_{73}^{-1} Mpc. Simulations of structure formation show that protoclusters originate from gravitationally collapsing regions as large as ∼20–40 Mpc at high redshift (e.g. Suwa, Habe & Yoshikawa 2006), and protocluster regions having sizes as large as these have been found in a number of cases (e.g. Campos et al. 1999; Shimasaku et al. 2003; Hayashino et al. 2004; Intema et al. 2006). It is possible that the [O III] emitters at $z \approx 3.10$ trace a subcluster that will eventually merge with the 'radio galaxy' protocluster at $z \approx 3.13$. Alternatively, the numbers of galaxies in the vicinity of overdense regions may be significantly enhanced relative to the general field due to an additional bias associated with the larger walls or filaments in which proto-clusters form. Such structures may have sizes of up to ∼100 Mpc on a comoving scale.

4.2 Ionization of [O III] emission

[O III] emission is commonly observed in the spectra of both star-forming and active galaxies. It is therefore interesting to consider

whether the emission from our [O III] excess galaxies at $z \sim 3.1$ is purely due to star-forming galaxies or whether there are contributions to their ionization by AGN. The comparison of the [O III] and *UV* continuum emission, and the morphology of the galaxies provide several interesting clues as to the origin of the [O III] emission. At low redshift the *UV* and optical continuum of star-forming galaxies containing an AGN is dominated by the stellar light (Kauffmann et al. 2003), while the emission lines are excited by both the AGN and the young stars. Therefore, objects for whose SFRs derived from [O III] emission are larger than those measured from their *UV* continua are likely to contain AGN that contribute to the ionization of the O^+ gas.

The SFRs derived from the [O III] luminosities are comparable to the SFRs derived from the *UV* continua for approximately half of the [O III] emitters. These [O III] galaxies all have clumpy morphologies in the ACS images and their [O III] emission is likely to be ionized by hot young stars. The radio galaxy and ID 8 have very extended clumpy structures that are suggestive of possible mergers or tidal streams. Five [O III] galaxies have [O III] fluxes that are formally larger by a factor >7 compared with the fluxes expected from their *UV*-derived SFRs, indicating that these galaxies harbour a hidden AGN. All five of these galaxies have compact core-dominated morphologies and ID 2 has a nearby companion galaxy. However, the uncertainties in the conversion between [O III] fluxes and SFR are large (factor of 3–4) and only in the cases of IDs 2 and 6 are the enhanced [O III] luminosities significant by greater than 3σ. If those two candidates are confirmed, the AGN fraction in this small field would be ~ 14 per cent of the total number of [O III] emitters compared with 5–10 per cent for the AGN overdensity in Lyα emitting galaxies in protoclusters at $z \sim 2$–4 (Pentericci et al. 2002; Croft et al. 2005) and 3–5 per cent for the AGN fraction in LBGs at $z \sim 3$ (Ouchi et al. 2008). Although the larger fraction of AGN in our [O III] small sample is only marginally significant, we note that this would be consistent with the fact that [O III] selection is known to be an efficient technique for finding low-luminosity AGN (type 2 Seyfert galaxies) in the optical (Zakamska et al. 2004). The conversion between SFR and [O III] luminosity is too uncertain to be able to make any strong conclusions as to the nature of the remaining three galaxies which have a larger [O III] luminosity than can be explained by star formation given their *UV* SFRs. We conclude that the [O III] galaxies detected at $z \approx 3.10$ are ionized by a mixture of young stars and AGN.

5 CONCLUSIONS AND FUTURE WORK

Searching for [O III] emitting galaxies is a new feasible method for detecting protocluster members. We have detected a new population of [O III] emitting galaxies in the neighbourhood of the radio galaxy MRC 0316−257 at $z = 3.13$. About half of the [O III] candidates emitters are LBGs and a third were also previously detected by the Lyα selection technique. The [O III] technique complements narrow-band searches using Lyα and Hα emission, and observations of the Lyman and Balmer breaks, for finding members of protoclusters. All of these different galaxy selection techniques are needed to study the different galaxy populations and to obtain a complete understanding of protocluster evolution. 13 candidate [O III] emitters were detected, including the radio galaxy, and eight of these were spectroscopically confirmed. Three [O III] emitting galaxies lie in a small redshift interval at $3.095 < z < 3.105$, which is blueshifted by $2100 \, \mathrm{km \, s^{-1}}$ with respect to the overdensity of Lyα emitting galaxies associated with the protocluster structure surrounding the radio galaxy. These three [O III] emitters may trace a substructure that lies

in front of the previously known 0316−257 protocluster. Further narrow-band imaging and spectroscopy of this field are necessary to establish the existence of such a structure. A possible explanation for the [O III]–Lyα redshift separation are the difference in the filter band pass together with the existence of a possible big superstructure around the radio galaxy. The observed space density of [O III] galaxies is consistent with the overdensity of 3.3 derived for Lyα galaxies in the MRC 0316−257 protocluster by Venemans et al. (2005) The detected [O III] candidate emitters exhibit a wide range of morphologies. About half have compact structures with an unresolved core on the *HST*-ACS image. All three spectroscopically confirmed [O III] emitters are compact. The median size of these objects is typically ≤ 0.24 arcsec, which at the average redshift $z = 3.11$ correspond to ~ 2 kpc. The remaining sources are clumpy, consistent with merging or interacting systems. Using the next generation of wide-field infrared imagers and spectrographs, it will be possible to increase the number of high-z detected [O III] emitters in the MRC 0316−257 by an order of magnitude and carry out comprehensive infrared studies of several protoclusters at high redshift. Not only will such observations result in greatly improved statistics, but also they will facilitate detailed mapping of the cosmic web at high redshifts.

REFERENCES

Bertin E., Arnouts S., 1996, A&AS, 117, 393
Blakeslee J. P., Anderson K. R., Meurer G. R., Benítez N., Magee D., 2003, in Payne H. E., Jedrzejewski R. I., Hook R. N., eds, ASP Conf. Ser. Vol. 295, Astronomical Data Analysis Software and Systems XII. Astron. Soc. Pac., San Francisco, p. 257
Bouwens R. J., Illingworth G. D., Blakeslee J. P., Broadhurst T. J., Franx M., 2004, ApJ, 611, L1
Calzetti D., Heckman T. M., 1999, ApJ, 519, 27
Calzetti D., Armus L., Bohlin R. C., Kinney A. L., Koornneef J., Storchi-Bergmann T., 2000, ApJ, 533, 682
Campos A., Yahil A., Windhorst R. A., Richards E. A., Pascarelle S., Impey C., Petry C., 1999, ApJ, 511, L1
Croft S., Kurk J., van Breugel W., Stanford S. A., de Vries W., Pentericci L., Röttgering H., 2005, AJ, 130, 867
De Breuck C., Reuland M., 2005, in Renzini A., Bender R., eds, Proc. ESO Workshop Multiwavelength Mapping of Galaxy Formation and Evolution. Springer-Verlag, Berlin, p. 374
Elmegreen D. M., 2007, in Combes F., Palous J., eds, Proc. IAU Symp. 235, Galaxy Evolution across the Hubble Time. Cambridge Univ. Press, Cambridge, p. 376
Fanelli M. N., O'Connell R. W., Thuan T. X., 1988, ApJ, 334, 665
Ferguson H. C., Dickinson M., Giavalisco M., Kretchmer C., Ravindranath S., Idzi R., Taylor E., Conselice C. J., 2004, ApJ, 600, L107
Ford H. C. et al., 1998, Proc. SPIE, 3356, 234
Giavalisco M., Livio M., Bohlin R. C., Macchetto F. D., Stecher T. P., 1996, AJ, 112, 369
Hatch N. A., Overzier R. A., Röttgering H. J. A., Kurk J. D., Miley G. K., 2008, MNRAS, 383, 931

Hawarden T. G., Leggett S. K., Letawsky M. B., Ballantyne D. R., Casali M. M., 2001, MNRAS, 325, 563

Hayashino T., Matsuda Y., Tamura H., Yamauchi R., Yamada T., Ajiki M., 2004, AJ, 128, 2073

Intema H. T., Venemans B. P., Kurk J. D., Ouchi M., Kodama T., Röttgering H. J. A., Miley G. K., Overzier R. A., 2006, A&A, 456, 433

Kauffmann G. et al., 2003, MNRAS, 346, 1055

Kennicutt R. C., Jr, 1992, ApJ, 388, 310

Kennicutt R., 1998, in Kaldeich B., ed., The Next Generation Space Telescope: Science Drivers and Technological Challenges, ESA SP-429. ESA, Noordwijk, p. 81

Kong X., Charlot S., Brinchmann J., Fall S. M., 2004, MNRAS, 349, 769

Kurk J., Venemans B., Röttgering H., Miley G., Pentericci L., 2004, in Plionis M., ed., Astrophys. Space Sci. Library Vol. 301, Multiwavelength Cosmology. Springer, Berlin, p. 141

Large M. I., Mills B. Y., Little A. G., Crawford D. F., Sutton J. M., 1981, MNRAS, 194, 693

Lee K.-S., Giavalisco M., Gnedin O. Y., Somerville R. S., Ferguson H. C., Dickinson M., Ouchi M., 2006, ApJ, 642, 63

Le Fevre O., Deltorn J. M., Crampton D., Dickinson M., 1996, ApJ, 471, L11

Lotz J. M., Madau P., Giavalisco M., Primack J., 2004, BAAS, 36, 1615

Lotz J. M., Madau P., Giavalisco M., Primack J., Ferguson H. C., 2006, ApJ, 636, 592

McCarthy P. J., Kapahi V. K., van Breugel W., Subrahmanya C. R., 1990, AJ, 100, 1014

Madau P., Pozzetti L., Dickinson M., 1998, ApJ, 498, 106

Meurer G. R., Heckman T. M., Leitherer C., Kinney A., Robert C., Garnett D. R., 1995, AJ, 110, 2665

Miley G. K., Overzier R. A., Tsvetanov Z. I., Bouwens R. J., Benítez N., Blakeslee J. P., Ford H. C., Illingworth G. D., 2004, Nat, 427, 47

Miley G. K. et al., 2006, ApJ, 650, L29

Monaco P., Møller P., Fynbo J. P. U., Weidinger M., Ledoux C., Theuns T., 2005, A&A, 440, 799

Moorwood A., Cuby J.-G., Biereichel P., Brynnel J., Delabre B., Devillard N., van Dijsseldonk A., 1998, The Messenger, 94, 7

Moorwood A., Cuby J.-G., Ballester P., Biereichel P., Brynnel J., Conzelmann R., Delabre B., Devillard N., 1999, The Messenger, 95, 1

Moorwood A. F. M., van der Werf P. P., Cuby J. G., Oliva E., 2000, A&A, 362, 9

Moustakas J., Kennicutt R. C., Jr, Tremonti C. A., 2006, ApJ, 642, 775

Mullis C. R., Rosati P., Lamer G., Böhringer H., Schwope A., Schuecker P., Fassbender R., 2005, ApJ, 623, L85

Oke J. B., 1974, in Reiz A., ed., Research Programmes for the New Large Telescopes. p. 29

Ouchi M. et al., 2004, in Mulchaey J. S., Dressler A., Oemler A., eds, in Carnegie Obs. Astrophys. Ser. Vol. 3, Clusters of Galaxies: Probes of Cosmological Structure and Galaxy Evolution. Cambridge Univ. Press, Cambridge, p. 41

Ouchi M. et al., 2008, ApJS, 176, 301

Overzier R. A. et al., 2006, ApJ, 637, 58

Overzier R. A., Bouwens R. J., Cross N. J. G., Venemans B. P., Miley G. K., Zirm A. W., Benítez N., 2008, ApJ, 673, 143

Pentericci L., Röttgering H. J. A., Miley G. K., McCarthy P., Spinrad H., van Breugel W. J. M., Macchetto F., 1999, A&A, 341, 329

Pentericci L., Kurk J. D., Carilli C. L., Harris D. E., Miley G. K., Röttgering H. J. A., 2002, A&A, 396, 109

Pettini M., Kellogg M., Steidel C. C., Dickinson M., Adelberger K. L., Giavalisco M., 1998, ApJ, 508, 539

Persson S. E., Murphy D. C., Krzeminski W., Roth M., Rieke M. J., 1998, AJ, 116, 2475

Seymour N. et al., 2007, ApJS, 171, 353

Shapley A. E., Steidel C. C., Pettini M., Adelberger K. L., 2003, ApJ, 588, 65

Shimasaku K. et al., 2003, ApJ, 586, L111

Spergel D. N. et al., 2003, ApJS, 148, 175

Stanford S. A. et al., 2005, ApJ, 634, L129

Stevens J. A. et al., 2003, Nat, 425, 264

Suwa T., Habe A., Yoshikawa K., 2006, ApJ, 646, L5

Teplitz H. I., Malkan M. A., McLean I. S., 1999, ApJ, 514, 33

Teplitz H. I. et al., 2000, ApJ, 542, 18

Venemans B. P. et al., 2005, A&A, 431, 793

Venemans B. P. et al., 2007, A&A, 461, 823

Vernet J., Fosbury R. A. E., Villar-Martín M., Cohen M. H., Cimatti A., di Serego Alighieri S., Goodrich R. W., 2001, A&A, 366, 7

Villar-Martín M. et al., 2006, MNRAS, 366, L1

Younger J. D. et al., 2007, ApJ, 671, 1241

Zakamska N. L., Strauss M. A., Ivezic Z., Schmidt G. D., 2004, BAAS, 36, 678

Zirm A. W. et al., 2005, ApJ, 630, 68

This paper has been typeset from a TEX/LATEX file prepared by the author.